JOC Article

Dioxadiazuliporphyrin: A Near-IR Redox Switchable Chromophore

Natasza Sprutta, Marta Siczek, Lechosław Latos-Grażyński,* Miłosz Pawlicki, Ludmiła Szterenberg, and Tadeusz Lis

Department of Chemistry, University of Wrocław, 14 F. Joliot-Curie Street, Wrocław 50 383, Poland

llg@wchuwr.chem.uni.wroc.pl

Received July 12, 2007

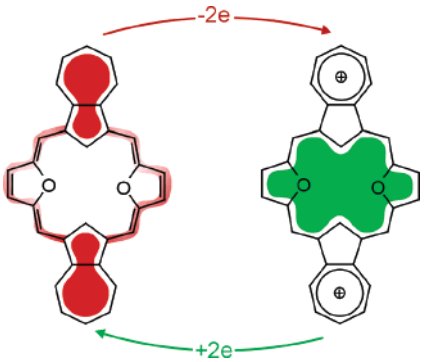

The synthesis of dioxadiazuliporphyrinogen **7** and its oxidized forms: dioxadiazuliporphyrin **8** and dication $\mathbf{8}^{2+}$, is reported. These compounds were characterized in solution using UV−vis and ^{1}H and ^{13}C NMR spectroscopic means and in the solid state via single-crystal X-ray diffraction analysis. Dioxadiazuliporphyrin is a nonaromatic porphyrinoid, readily and reversibly oxidizable to its cation radical and to the aromatic carbaporphyrinoid dication, which can be viewed as a 21,23-dicarba-22,24-dioxaporphyrin with two fused tropylium rings. Further insight into the geometric and magnetic manifestations of aromaticity and antiaromaticity in the case of the redox couple **8**, $\mathbf{8}^{2+}$ is obtained using density functional calculations and nucleus-independent chemical shifts.

Introduction

Molecules containing extended π-electron chromophores are of interest because of their potential for applications in optoelectronics, electrochromic, or molecular conductivity.[1,2] These applications necessitate systems with unique electronic features, such as near-infrared absorptions, high extinction coefficients, or small HOMO−LUMO gaps.[3−9] To achieve these requested molecular properties, combinations of different structural motifs involving azulene can be tested.[5,6,10−12] One of the recently explored concepts of chromophore construction involves combining azulene rings with porphyrin or porphyrinoid frameworks.[6,13] Azulene, the nonalternant isomer of naphthalene, is a uniquely flexible π-electron system, which can act as an electron donor or acceptor, depending on the way it is incorporated into the molecule. For instance, the azulene motif has been used for peripheral substitution of porphyrins, yielding highly conjugated systems with large two-photon absorption cross sections.[6]

(1) Monk, P. M. S.; Mortimer, R. J.; Rosseinsky, D. R. *Electrochromism: Fundamentals and Applications;* VCH: Weinheim, Germany 1995.
(2) Coronado, E.; Galán-Macarós, J. R. *J. Mater. Chem.* **2005**, *15*, 66.
(3) Gill, S. H.; Harmjanz, M.; Sanyamara, J.; Finger, I.; Scott, M. J. *Angew. Chem., Int. Ed.* **2004**, *43*, 485.
(4) Kumar, R.; Misra, R.; Chandrashekar, T. K.; Suresh, E. *Chem. Commun.* **2007**, 43.
(5) Lambert, C.; Nöll, G.; Zabel, M.; Hampel, F.; Schmälzlin, E.; Brauchle, C.; Meerholz, K. *Chem.−Eur. J.* **2003**, *9*, 4232.
(6) Kurotobi, K.; Kim, K. S.; Noh, S. B.; Kim, D.; Osuka, A. *Angew. Chem., Int. Ed.* **2006**, *45*, 3944.
(7) Chou, J.-H.; Nalwa, H. S.; Kosal, M. E.; Rakow, N. A.; Suslick, K. S. Applications of Porphyrins and Metalloporphyrins to Materials Chemistry. In *The Porphyrin Handbook;* Kadish, K. M., Smith, K. M., Guilard, R., Eds.; Academic Press: San Diego, CA, 2000; p 43.
(8) Yoon, D. H.; Lee, S. B.; Yoo, K.-H.; Kim, J.; Lim, K. J.; Aratani, N.; Tsuda, A.; Osuka, A.; Kim, D. *J. Am. Chem. Soc.* **2003**, *125*, 11062.
(9) Seidel, D.; Lynch, V.; Sessler, J. L. *Angew. Chem., Int. Ed.* **2002**, *41*, 1422.
(10) Okazaki, T.; Laali, K. K. *Org. Biol. Chem.* **2003**, *1*, 3078.
(11) Wakabayashi, S.; Kato, Y.; Mochizuki, K.; Suzuki, R.; Matsumoto, M.; Sugihara, Y.; Shimizu, M. *J. Org. Chem.* **2007**, *72*, 744.
(12) Ito, S.; Akimoto, K.; Kawakami, K.; Tajiri, A.; Shoji, T.; Satake, K.; Morita, N. *J. Org. Chem.* **2007**, *72*, 162.
(13) Sprutta, N.; Swiderska, M.; Latos-Grażyński, L. *J. Am. Chem. Soc.* **2005**, *127*, 13108.

10.1021/jo7015218 CCC: $37.00
Published on Web 11/15/2007

CHART 1

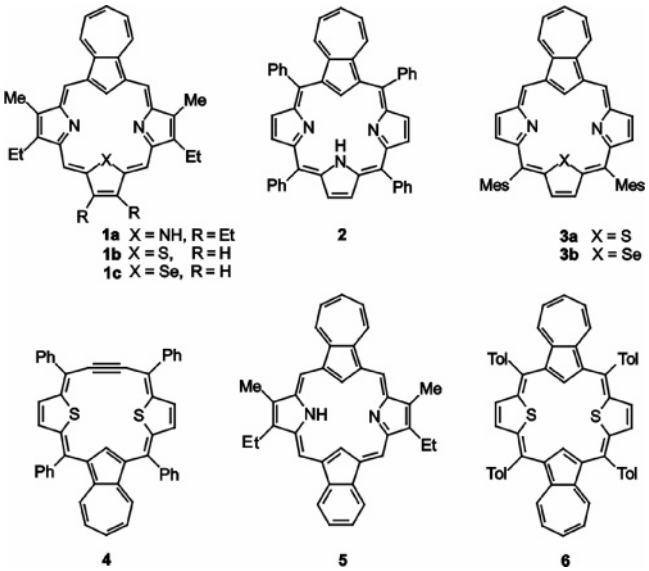

In an earlier approach, the azulene moiety was employed to replace the constituent pyrrole rings of the porphyrin macrocycle. To date, a number of different systems have been reported, including variously substituted azuliporphyrins (**1a**, **2**)[14−20] (Chart 1), their heteroanalogues containing thiophene (**1b**, **3a**) or selenophene (**1c**, **3b**),[21] and eventually hybrid systems such as benzocarbaazuliporphyrin (**5**)[18] or dithiaethyneazuliporphyrin (**4**).[22] The incorporation of azulene as the key structural unit leads to systems exhibiting borderline macrocyclic aromaticity and unusual reactivity pathways. Some of these systems were shown to coordinate metal ions in a porphyrin-like manner, resulting in metalation of the azulene ring.[16,20,22]

Recently, we reported an efficient synthesis of a hybrid thiophene−azulene macrocycle (**6**) and described its redox chemistry.[13] This new system showed a number of easily attainable oxidation states with widely differing electronic absorption spectra and was considered as a potential element for the construction of electrochromic materials.

Encouraged by the interesting spectroscopic and electrochemical properties determined for **6**, we have decided to explore some structural modifications potentially capable of fine-tuning the properties of the diazuliporphyrin core. Actually, one can control the overall properties of porphyrinoids by applying well-planned peripheral substitutions. Thus, a remote functionalization of *meso*-aryl rings or the more direct substitution at β-pyrrole positions may offer suitable means of fine adjustments.

SCHEME 1. Synthetic Route

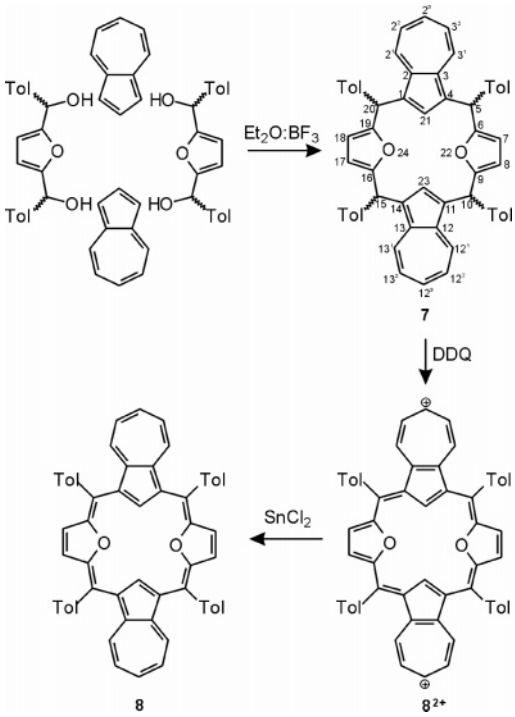

Apart from peripheral substitution, the fundamentally different method, involving core alteration, has been considered as an independent route of adjustment as previously explored in the class of heteroporphyrins.[23,24]

Thus, we have attempted to elucidate the influence of the incorporation of two furan rings into a structural framework analogous to that of **6**. Here, we report on the synthesis, structure, as well as electrochemical and spectroscopic properties of dioxadiazuliporphyrin. In particular, we comment on the relationship between its oxidation states and the corresponding ^{1}H NMR spectroscopic patterns.

Results and Discussion

Synthesis of Macrocycles. Dioxadiazuliporphyrinogen **7** was obtained in a modification of the synthesis described for tetraaryl-21,23-diheteroporphyrins.[23,25] This method relies on the known suitability of azulene as a substrate in the Rothemund-type condensation[17,26,27] (Scheme 1) and was previously applied for the synthesis of dithiadiazuliporphyrinogen.[13] **7** was invariably obtained as a mixture of stereoisomers with a total yield of 91%.

Chart 2 shows the five possible stereoisomers of **7** (excluding the enantiomers of the chiral isomers **7d** and **7e**) and indicates their effective symmetry in solution, expected in the case of full conformational flexibility. Interestingly, the multiplicities of all resonances should be identical for **7a**, **7b**, **7c**, and **7d**, making these four species indistinguishable by the symmetry of their ^{1}H NMR spectrum. In particular, regardless of its

(14) Lash, T. D. *Chem. Commun.* **1998**, 1683.
(15) Lash, T. D.; Chaney, S. T. *Angew. Chem., Int. Ed.* **1997**, *36*, 839.
(16) Graham, S. R.; Ferrence, G. M.; Lash, T. D. *Chem. Commun.* **2002**, 894.
(17) Colby, D. A.; Lash, T. D. *Chem.−Eur. J.* **2002**, *8*, 5397.
(18) Graham, S. R.; Colby, D. A.; Lash, T. D. *Angew. Chem., Int. Ed.* **2002**, *41*, 1371.
(19) Lash, T. D.; Colby, D. A.; Graham, S. R.; Ferrence, G. M.; Szczepura, L. F. *Inorg. Chem.* **2003**, *42*, 7326.
(20) Colby, D. A.; Ferrence, G. M.; Lash, T. D. *Angew .Chem., Int. Ed.* **2004**, *43*, 1346.
(21) Venkatraman, S.; Anand, V. G.; PrabhuRaja, H.; Rath, H.; Sankar, J.; Chandrashekar, T. K.; Teng, W.; Senge, K. R. *Chem. Commun.* **2002**, 1660.
(22) Berlicka, A.; Sprutta, N.; Latos-Grażyński, L. *Chem. Commun.* **2006**, 3346.
(23) Latos-Grażyński, L. Core Modified Heteroanalogues of Porphyrins and Metalloporphyrins. In *The Porphyrin Handbook;* Kadish, K. M., Smith, K. M., Guilard, R., Eds.; Academic Press: New York, 2000; p 361.
(24) Gupta, I.; Ravikanth, M. *Coord. Chem. Rev.* **2006**, *250*, 468.
(25) Chmielewski, P. J.; Latos-Grażyński, L.; Olmstead, M. M.; Balch, A. L. *Chem.−Eur. J.* **1997**, *3*, 268.
(26) Asao, T.; Ito, S.; Morita, N. *Tetrahedron Lett.* **1988**, *29*, 2839.
(27) Colby, D. A.; Lash, T. D. *J. Org. Chem.* **2002**, *67*, 1031.

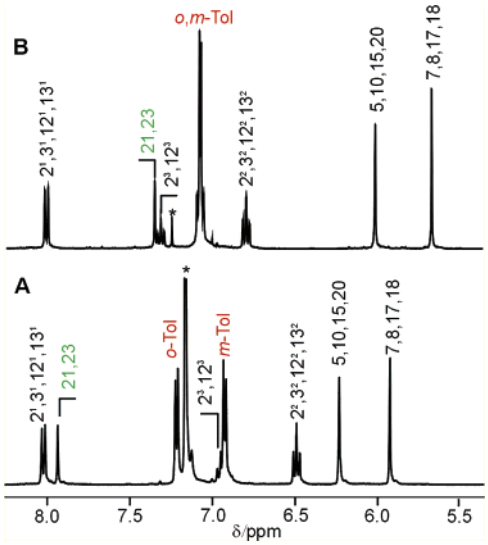

FIGURE 1. ^{1}H NMR spectra of (A) **7a** in C_6D_6 (298 K) and (B) **7a** in $CDCl_3$ (298 K).

CHART 2

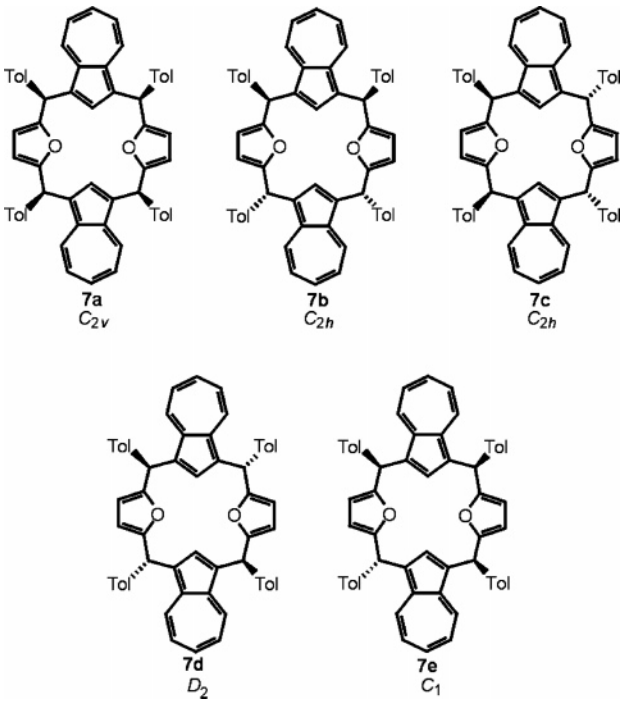

effective symmetry (C_{2v}, C_{2h}, or D_2), each of these systems will display a single set of resonances corresponding to the azulene unit (a doublet and two triplets with the relative intensity ratio of 2:2:1) accompanied by a singlet corresponding to the furan ring. On the contrary, stereoisomer **7e**, which has no element of symmetry, should be characterized by two AB spin systems of the furan β-protons and two ABCDE spin systems of the azulene rings.

Compound **7a** was separated from the mixture by fractional crystallization, and its stereochemistry was proved by X-ray diffraction (see below). By comparing the ^{1}H NMR spectrum of the pure isomer (Figure 1) with that of the isomeric mixture (Figure 2), it was established that **7a** was the major condensation product. As discussed earlier, the ^{1}H NMR spectrum of **7a** is consistent with the C_{2v} symmetry (Figure 1). The signals of

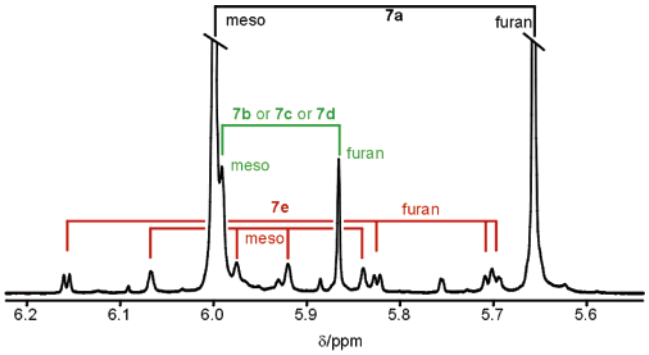

FIGURE 2. Partial ^{1}H NMR spectrum of a mixture of isomers **7a**−**7e** ($CDCl_3$, 298 K).

azulene and furan rings are in regions expected of a porphyrinogen-like structure devoid of a macrocyclic conjugation. Subsequently, it was found that the positions of resonances are solvent-dependent. The effect is most pronounced for the signal of inner azulene protons (21,23-H), which appears at 7.35 ppm when measured in $CDCl_3$ and at 7.91 ppm in C_6D_6. Additionally, the difference of chemical shifts between the ortho and meta signals of the *p*-tolyl substituents is increased in the C_6D_6 solution.

An analysis of the ^{1}H NMR spectrum (Figure 2) of the porphyrinogen mixture as obtained directly from the condensation allowed the straightforward identification of the resonances assigned to **7a** and asymmetric **7e**. Their relative contributions equal 62 and 19%, respectively (as determined by integration of ^{1}H NMR signals, Figure 2). An unambiguous spectroscopic identification of **7e** is possible because of its peculiar symmetry. The characteristic two AB systems of furan protons ($^3J = 3.3$ Hz) are present on NMR spectrum of **7e**. Careful comparison of the relative intensities allowed the selection of four resonances, which belong to the four *meso*-H positions. The remaining set has been related to a single albeit not determined species (**7b**, **c**, or **d**, 17%).

It is important to notice that in the case of dithiadiazuliporphyrinogen the mixture of isomers was also obtained, but their ratio was drastically changed. Significantly, thiophene analogue of **7b** was the major condensation product[14] (for more information, see Supporting Information, Figure S1).

Although a condensation of azulitripyrran and 2,5-furandicarbaldehyde failed to give any isolatable meso-unsubstituted oxaazuliporphyrin and only oxacarbaporphyrins were isolated,[18] oxidation of **7** (isomers mixture or pure **7a**) with excess (8 equiv) of 2,3-dichloro-5,6-dicyano-*p*-benzoquinone (DDQ) led to the practically quantitative formation of the dication $\mathbf{8}^{2+}$ (Scheme 1), which could be quantitatively reduced to **8** by $SnCl_2$ in THF. Actually, the oxidation of **8** with dibromine (excess) on a synthetic scale allowed isolation of $[\mathbf{8}^{2+}](Br_3)_2$.

Crystal Structure of Dioxadiazuliporphyrin and Its Porphyrinogen. The X-ray structures of **7a** and **8** were obtained (Figure 3).

Porphyrinogen **7a** adopts a saddle conformation in the solid state with the azulene and furan rings tilted in opposite directions. Thus, the angle between two furan rings equals 20.6°, whereas the corresponding dihedral angle between azulene planes equals 72.8°. The molecular geometry is clearly described by the dihedral angles between the C_4 plane (defined by the four meso carbons) and azulene (54.9° and 52.3°) or furan (79.3°and 80.1°) planes, respectively. Bond lengths in the

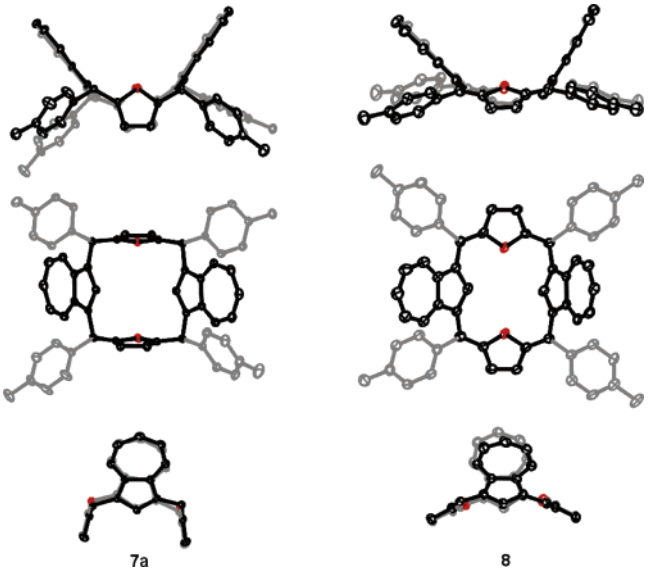

FIGURE 3. Crystal structures of **7a** and **8**. Hydrogen atoms and solvent molecules are omitted for clarity. Fragments pointing away from the viewer are shown in gray. In the bottom projections, the meso substituents are omitted for clarity.

azulene and furan fragments of **7a** are close to those in isolated molecules (Table S2 in Supporting Information).

In the solid state, **8** adopts saddle conformation. The dihedral angle between two furan rings and azulenes for **8** equals 53.0° and 76.2°, respectively (Figure 3). Dihedral angles between each furan and C_4 plane equal 24.7° and 28.3°, respectively, whereas the dihedral angles between each of the azulene moieties and the C_4 plane are 43.6° and 60.2°. The azulene rings are making room for the adjacent *meso*-aryls, which tend to be almost coplanar with the furan moieties. The peculiar orientation of the *meso*-aryl rings is readily reflected by the dihedral angle between the respective C_6 and $C_{4(meso)}$ planes: *p*-tolyl(5) 24.1°; *p*-tolyl(10) 26.3°; *p*-tolyl(15) 30.8°; *p*-tolyl(20) 23.9°.

There is an appreciable effect of the conjugation on the furan fragment. The bond distances within the furan ring are altered in accord with the valence bond structure of **8**. Thus, the $C_\alpha-C_\beta$ bond lengths (1.432(4), 1.430(3), 1.430(3), 1.436(3) Å) are longer than the $C_\beta-C_\beta$ distances (1.353(3), 1.358(3) Å), whereas the reverse is true for porphyrinogen **7a**. Similarly, the $C_{meso}-C_\alpha$ (furan) bonds (1.348(3), 1.365(3), 1.348(3), 1.364(3) Å) reflect some double-bond character, while the $C_{meso}-C_\alpha$ (azulene) distances (1.475(3), 1.466(3), 1.462(3), 1.476(3) Å) approach the $C(sp^2)-C(sp^2)$ single-bond limit. In both **7a** and **8**, the geometry of azulene moieties remains largely unaltered, suggesting that they are not conjugated with the macrocycle (Table S2 in Supporting Information).

Redox Characterization of Dioxadiazuliporphyrin. Systematic titration of **8** with Br_2, followed by UV−vis spectroscopy, revealed the presence of an intermediate species $\mathbf{8}^{\bullet+}$ before formation of the final dication $\mathbf{8}^{2+}$ (Scheme 2).

These three species constitute a multielectron redox system. There are only a few other examples of porphyrinoids for which two different oxidation states (isophlorin and dication) could be isolated: tetrathiaporphyrin, its oxa-congener,[28−30] and the dithiadiazuliporphyrin and its dication[13] are among them. During oxidation, the color of the solution changes from wine-red (**8**), to orange ($\mathbf{8}^{\bullet+}$), to orange-pink ($\mathbf{8}^{2+}$). The redox system comprising **8**, $\mathbf{8}^{\bullet+}$, and $\mathbf{8}^{2+}$ has been investigated using chemical and physical methods.

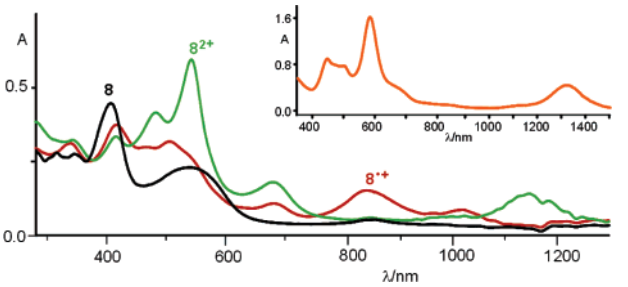

FIGURE 4. UV−vis absorption spectra (CH_2Cl_2, 298 K) of **8** (black), $\mathbf{8}^{\bullet+}$ (red), and $\mathbf{8}^{2+}$ (green). The spectra were obtained by titrating **8** with Br_2 in CH_2Cl_2 solution. Inset (orange) presents the spectrum of the dithiadiazuliporphyrin dication $\mathbf{6}^{2+}$.

SCHEME 2. Oxidation of Dioxadiazuliporphyrin

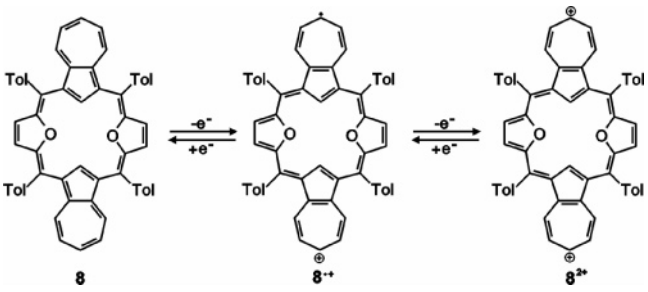

A stepwise one-electron oxidation of **8** produces remarkable changes in the electronic spectra as illustrated at Figure 4. The formation of the radical $\mathbf{8}^{\bullet+}$ is accompanied by two bands rising in the NIR region (i.e., 833 and 1020 nm). The next redox step yields a band at 1148 nm. To the best of our knowledge, this large bathochromic shift is near the largest one reported for monomeric porphyrins, that is, for a quadruply azulene-fused porphyrin (λ = 1136 nm).[6] Correspondingly, copper(II) and palladium(II) complexes of perfectly planar porphyrins, bearing bis(naphthoazulenone) ring systems, exhibit the longest absorption wavelength reported for monomeric metalloporphyrins (palladium(II) porphyrin, λ = 994 and 1145 nm; copper(II) porphyrin, λ = 1038 and 1204 nm).[3] Only the absorptions of triply fused, multiporphyrin tapes reach further into the IR region.[31] Recently described 22-hydroxybenziporphyrin revealed also interesting absorption in the NIR region once converted to its diprotonated form (920 nm).[32]

One can readily notice that the general spectral changes resemble closely those described previously for the dithiadiazuliporphyrin redox system, albeit for each given oxidation state the corresponding dithiaporphyrin band is bathochromic shifted.[13] Thus, the intense band at 850 nm extending its intensity until 1000 nm was reported for $\mathbf{6}^{\bullet+}$. This observation led us to reexamine the dithidiazuliporphyrin dication spectrum exploring the NIR region. It allowed a detection of the NIR band at 1320

(28) Vogel, E.; Haas, W.; Knipp, B.; Lex, J.; Schmickler, H. *Angew. Chem., Int. Ed.* **1988**, *27*, 406.
(29) Vogel, E.; Röhrig, P.; Sicken, M.; Knipp, B.; Herrmann, A.; Pohl, M.; Schmickler, H.; Lex, J. *Angew. Chem., Int. Ed.* **1989**, *28*, 1651.
(30) Vogel, E.; Fröde, C.; Breihan, A.; Schmickler, H.; Lex, J. *Angew. Chem., Int. Ed.* **1997**, *36*, 2609.
(31) Cho, H. S.; Jeong, D. H.; Cho, S.; Kim, D.; Matsuzaki, Y.; Tanaka, K.; Tsuda, A.; Osuka, A. *J. Am. Chem. Soc.* **2002**, *124*, 14642.
(32) Stępień, M.; Latos-Grażyński, L.; Szterenberg, L. *J. Org. Chem.* **2007**, *72*, 2259.

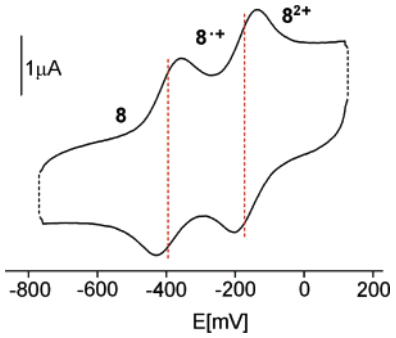

FIGURE 5. Cyclic voltammogram of **8** (CH_2Cl_2 solution, supporting electrolyte TBAP; working electrode, glassy carbon disk; reference electrode, Ag/AgCl; $E_{1/2}$ for ferrocene 0 mV).

nm. At this point, one can comment that the dithiadiazuliporphyrin dication provides the lowest energy electronic transitions ever observed for a chromophore confined in the porphyrin-like frame.

The solution of $\mathbf{8}^{\bullet+}$ (obtained by titration of dichloromethane solution of **8** with Br_2/CH_2Cl_2) exhibits a single line at $g = 2.0028$ (CH_2Cl_2, 298 K), consistent with the cation radical electronic structure. Cyclic voltammetry (Figure 5) demonstrates that **8** undergoes two consecutive, semireversible one-electron oxidations with half-wave potentials of (1) −394 mV and (2) −173 mV (if half-wave potential of ferrocene equals 0 mV), yielding $\mathbf{8}^{\bullet+}$ and $\mathbf{8}^{2+}$, respectively. These potentials are even lower than those for their thia analogues (−326 and −113 mV),[13] which accounts for the easy accessibility of the oxidized forms.

NMR Studies. Well-resolved ^{1}H NMR spectra of **8** and $\mathbf{8}^{2+}$ can be obtained under carefully controlled conditions. In each case, the presence of even a minute amount of the radical $\mathbf{8}^{\bullet+}$ leads to significant line broadening, which confirms the fast exchange between the differently oxidized forms **8**, $\mathbf{8}^{\bullet+}$, and $\mathbf{8}^{2+}$.[33] The pertinent equilibria are solvent-dependent: $\mathbf{8}^{2+}$ yields narrow lines in more polar solvents, such as acetonitrile-d_3 (Figure 6C), whereas in chloroform the spectrum is very broad. Conversely, poor solubility of the charged forms $\mathbf{8}^{\bullet+}$ and $\mathbf{8}^{2+}$ in benzene or toluene results in the desired sharpening of the spectrum of **8** in these solvents (Figure 6B).

^{1}H chemical shifts observed for $\mathbf{8}^{2+}$, in particular the peculiar upfield position of the inner 21,23-H protons (−0.39 ppm), show that a diatropic ring current is present in the macrocycle. In fact, $\mathbf{8}^{2+}$ can be treated as a 21,23-dicarba-22,24-dioxaporphyrin with two fused tropylium rings (Scheme 3).

DFT Calculations and the Electronic Structure. Density functional theory (DFT) has been successfully used to describe the properties of porphyrins and related systems, providing information on their energetics, conformational behavior, tautomerism, and aromaticity.[34] We have previously applied DFT modeling to study the relationship between aromaticity and tautomerism of 2-oxybenziporphyrin[35] and 22-hydroxybenziporphyrin.[33]

(33) Swift, T. J. The Paramagnetic Linewidth. In *NMR of Paramagnetic Molecules. Principles and Applications*; La Mar, G. N., Horrocks, W. D., Jr., Holm, R. H., Eds.; Academic Press: New York, 1973; pp 53−83.

(34) Ghosh, A. Quantum Chemical Studies of Molecular Structures and Potential Energy Surafaces of Porphyrins and Hemes. In *The Porphyrin Handbook;* Kadish, K. M., Smith, K. M., Guilard, R., Eds.; Academic Press: San Diego, CA, 2000; p 1.

(35) Stępień, M.; Latos-Grażyński, L.; Lash, T. D.; Szterenberg, L. *Inorg. Chem.* **2001**, *40*, 6892.

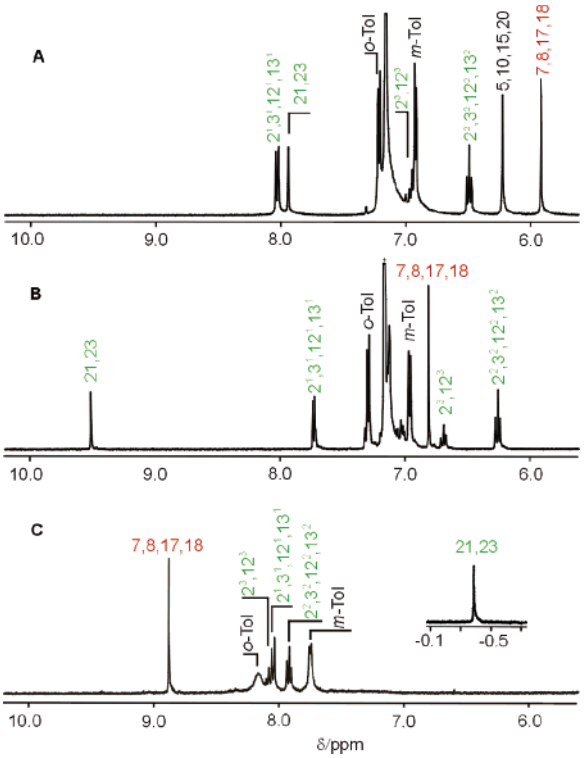

FIGURE 6. ^{1}H NMR spectra of (A) **7a** (C_6D_6, 298 K), (B) **8** (C_6D_6, 298 K), and (C) $\mathbf{8}^{2+}$ (CD_3CN, 298 K).

SCHEME 3. Conjugation Pathway for $\mathbf{8}^{2+}$

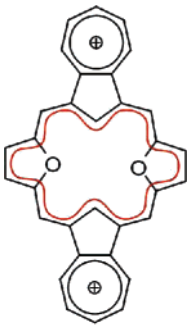

$\mathbf{8}^{2+}$

While the magnetic manifestations of aromaticity or antiaromaticity can be observed using ^{1}H NMR spectroscopy, this method does not provide detailed information on the energetic and structural consequences of electron delocalization in these two species. To address these issues, we carried out DFT calculations performing full geometry optimizations at the B3LYP/6-31G** level. To explore the role of the heteroatom (oxygen versus sulfur), analogous calculations were carried out for dithiadiazuliporphyrin **6** and its dication $\mathbf{6}^{2+}$ (Supporting Information). In addition, to probe the effect of meso substitution on the chemical shifts of the protons attached to the macrocycle, meso-unsubstituted variants of $\mathbf{8}^{2+}$ and **8** ($\mathbf{9}^{2+}$ and **9**, respectively) were also modeled.

The DFT-optimized geometries of structures $\mathbf{8}^{2+}$ and **8** are shown in Figure 7. In each case, the macrocycle adopts a saddle conformation. Despite the different oxidation state, the puckering of the macrocycle is nearly identical in **8** and $\mathbf{8}^{2+}$. The out-of-plane orientation of the azulene rings enables the *meso*-aryl substituents to be almost coplanar with the adjacent furan rings. The DFT-optimized structure of **8** is very similar to those

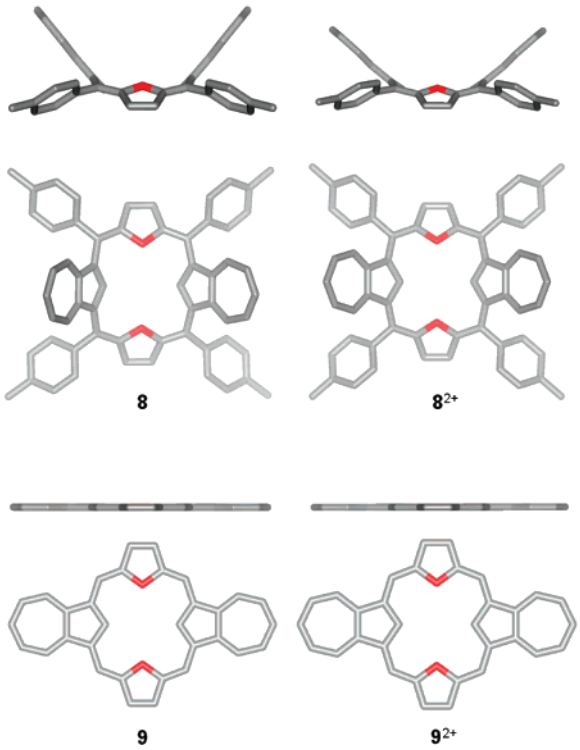

FIGURE 7. DFT-optimized geometries (B3LYP/6-31G**) of **8**, $\mathbf{8}^{2+}$, **9**, and $\mathbf{9}^{2+}$ (side and top views).

determined by X-ray crystallography (Figure 3). The bond distances involving the meso bridges and the furan rings indicate that this part of the macrocycle is highly conjugated. Still the azulene moieties preserve the typical bond lengths of free azulene. In accord with that observation, the $C_{\alpha(azulene)}-C_{meso}$ bond distances are typical for $C(sp^2)-C(sp^2)$ single bonds.

Similarly to the dithiadiazuliporphyrin cation $\mathbf{6}^{2+}$,[14] the furan analogue $\mathbf{8}^{2+}$ displays macrocyclic aromaticity, which has an effect on the ^{1}H NMR spectrum. The observed diatropic ring current can be explained by assuming an [18]annulenoid delocalization pathway shown in Scheme 3, which excludes the oxygen atoms and the seven-membered rings of the azulenes. In this model, similar to previous descriptions of other azuliporphyrins,[16,22] the positive charge is distributed in the seven-membered rings, which can be viewed as tropylium cations fused to the periphery of the macrocycle.

The optimized geometry of $\mathbf{8}^{2+}$ (Figure 8) shows no bond localization, as expected of an aromatic [$4n + 2$]annulenoid system.

According to the Hückel aromaticity rules, it could be reasoned that **8**, the two-electron-reduced form of $\mathbf{8}^{2+}$, should be antiaromatic. The 21,23-H signal of **8** is shifted downfield to 9.54 ppm, in agreement with the expected effect of macrocyclic paratropicity. Unfortunately, the rest of the ^{1}H NMR spectrum of **8** cannot be taken as a conclusive proof of antiaromaticity, because the required upfield shifts of peripheral signals are either absent or too small to be interpretable. This apparent lack of well-defined antiaromatic character can be explained by considering possible conjugation pathways in **8** (Scheme 4). In the dominant delocalization scheme (**8**-1), which is undoubtedly preferred for its lack of charge separation, cyclic conjugation is restricted to azulene rings. Other delocalization schemes necessitate charge separation, which makes them much less feasible. Mode **8**-2 directly corresponds to the delocalization

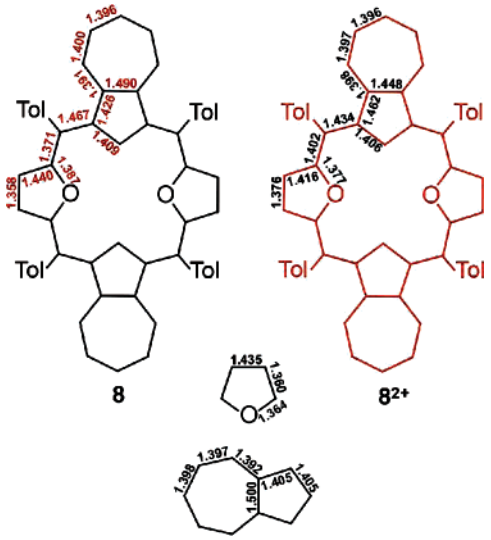

FIGURE 8. Bond distances calculated for **8**, $\mathbf{8}^{2+}$, azulene, and furan rings (DFT, B3LYP/6-31G**). Data for **6**, $\mathbf{6}^{2+}$, **9**, and $\mathbf{9}^{2+}$ are provided in the Supporting Information.

SCHEME 4. Possible Conjugation Pathways for 8

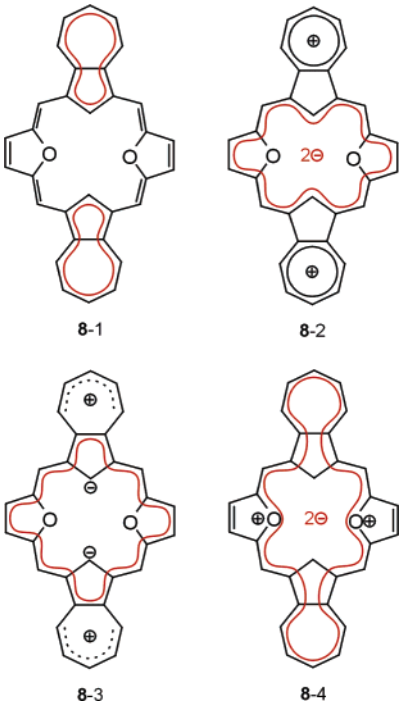

scheme described for $\mathbf{8}^{2+}$, with the two additional electrons introduced to the macrocyclic circuit while preserving the tropylium character of the seven-membered rings.

The following delocalization scheme (**8**-3) makes use of the zwitterionic forms known to contribute to the structure of the isolated azulene ring. Here the negative charges are localized at positions 21,23, whereas the positive charges are distributed on the outer part of the seven-membered rings. The remaining electrons form a 20-electron macrocyclic circuit. Finally, a 28-electron circular pathway can be considered (**8**-4), which encompasses the entire molecule, excluding positions 21,23 and the peripheral atoms of the furan rings (7,8,17,18).

As described earlier (Figure 4), the oxidation of diheterodiazuliporphyrins was accompanied by characteristic bands in the

NIR region of the electronic spectrum. The DFT calculation demonstrated that HOMO−LUMO gaps in the series studied decrease markedly as oxidation state of macrocycle increases (17104, 10517, 15576, and 9566 cm^{-1} for **8**, $\mathbf{8}^{2+}$, **6**, and $\mathbf{6}^{2+}$, respectively). Actually, the HOMO−LUMO split correlates with positions of the lowest energy band in UV−vis electronic spectra of dioxadiazuliporphyrin and dithiadiazuliporphyrin redox systems.

NICS and Chemical Shift Calculations. Nucleus-independent chemical shifts (NICS) have been proposed by Schleyer et al. as a computational measure of aromaticity that is related to experimental magnetic criteria.[36,37] NICS is defined as the negative shielding value computed at the geometric center of a ring. For monocyclic systems, NICS values generally correlate well with other established aromaticity criteria[36,37] (the validity of these correlations was, however, disputed[38−40]), but they are less conclusive for polycyclic molecules. Nevertheless, the NICS method has been used to assess the aromaticity of porphyrins[41,42] and their analogues.[32,43] It has been argued that NICS values should be used only as descriptors of local aromaticity and not to quantify the aromaticity of the entire molecule.[44] Bearing this restriction in mind, we decided to perform a NICS analysis for diheterodiazuliporphyrins and their dications (meso-substituted and -unsubstituted) and compare the results with the experimental data.

NICS values were calculated for molecules **8**, $\mathbf{8}^{2+}$ and **6**, $\mathbf{6}^{2+}$ at the centers of the seven- and five-membered ring of azulene and the two furan or thiophene rings. In addition, the NICS value for the central 16-membered ring (center ring) was obtained in each case. The results are depicted in Figure 9 (data for **6** and $\mathbf{6}^{2+}$, which yielded essentially similar results, are included in the Supporting Information). The two systems, **8** and $\mathbf{8}^{2+}$, despite having similar geometries, exhibit markedly different NICS signatures. For the aromatic system $\mathbf{8}^{2+}$, the central NICS values are negative and comparable with that reported for porphyrin[41] or 2-oxobenziporphyrin.[32] On the other hand, for the effectively nonaromatic form **8** this NICS value is small in magnitude (+1.47 ppm), indicating that the macrocyclic aromaticity is not well defined. For comparison, for the antiaromatic 22-oxybenziporphyrin, the center ring NICS is +5.0 ppm.[32] Furthermore, the pattern of NICS values in the C_7 and C_5 rings of the azulene moieties in **8** is similar to that in free azulene, indicating that they are only weakly interacting with the rest of the macrocycle. On the contrary, the NICS value of the azulene C_5 ring in $\mathbf{8}^{2+}$ is significantly elevated, corresponding to the disruption of local aromaticity by extensive macrocyclic conjugation. A similar analysis can be performed for the furan rings: the cross-conjugated C_4O subunits in **8** show NICS values that are much higher than the corresponding shift calculated for isolated furan. On the other hand, the furan NICS values obtained for $\mathbf{8}^{2+}$ may be explained as resulting from the aromaticity of the macrocycle.

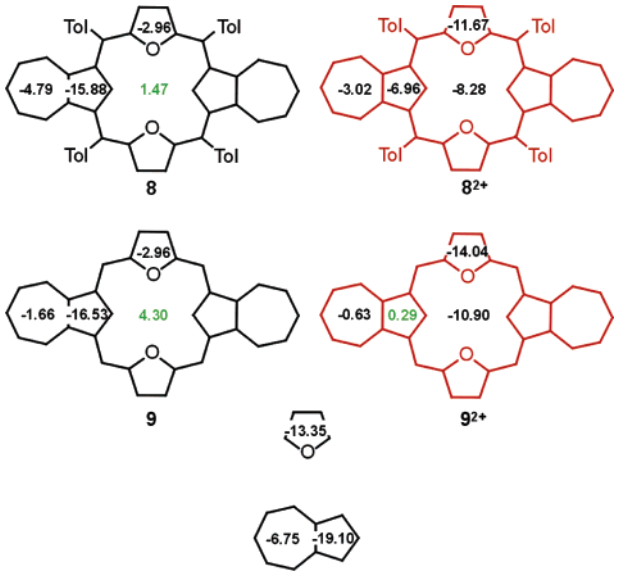

FIGURE 9. NICS (B3LYP/6-31G**) calculated for **8**, $\mathbf{8}^{2+}$ (for data for **6**, $\mathbf{6}^{2+}$, see Supporting Information).

TABLE 1. Experimental and Calculated ^{1}H NMR Shifts (ppm)

group of protons	**8**[a]	**8**[b]	**9**[b]	$\mathbf{8}^{2+a}$	$\mathbf{8}^{2+b}$	$\mathbf{9}^{2+b}$
7, 8, 17, 18	6.80	6.66	5.96	8.90	8.95	10.08
2^1, 3^1, 12^1, 13^1	7.73	7.65	7.42	8.06	8.10	10.00
2^2, 3^2, 12^2, 13^2	6.24	6.58	6.41	7.93	7.78	9.08
2^3, 12^3	6.68	7.26	7.18	8.10	8.09	9.09
21, 23	9.54	10.26	12.44	−0.39	−1.32	−3.74
o-Tol	7.29	7.16		8.17	8.16	
m-Tol	6.95	7.10		7.76	8.12	
CH_3	2.12	2.19		2.70	2.85	

[a] Experimental data. [b] Calculated data.

Structures **9** and $\mathbf{9}^{2+}$ display NICS values that are different from those calculated for the substituted forms **8** and $\mathbf{8}^{2+}$. This difference results from the planarity of **9** and $\mathbf{9}^{2+}$ and from the absence of *meso*-aryl substituents, whose ring currents contribute to the calculated chemical shifts. As a consequence, the macrocyclic aromaticity of the dioxadiazuliporphyrin dication, measured with the value of the center ring NICS, is more pronounced in $\mathbf{9}^{2+}$ than in $\mathbf{8}^{2+}$. Interestingly, the center ring NICS in **9** is fairly high (4.30 ppm), indicating that residual paratropicity might indeed be present in neutral dioxadiazuliporphyrin. ^{1}H NMR chemical shifts calculated for **8**, $\mathbf{8}^{2+}$ using the B3LYP method are given in Table 1. The table includes the chemical shifts calculated for *meso*-aryl free structures as well. Analogous calculations were performed for **6** and $\mathbf{6}^{2+}$ (the data, with corrected assignment of 21,23-H and thiophene protons signals, are included in the Supporting Information).

There is a good agreement between calculated and experimental shifts, even though the paratropicity of **8** and the diatropicity of $\mathbf{8}^{2+}$ are significantly exaggerated. This effect is likely due to the known propensity of the B3LYP functional to overestimate π-conjugation.[45] Nevertheless, there is a good linear correlation between the calculated and experimental shifts of **8** and $\mathbf{8}^{2+}$ (graphs are included in Supporting Information).

(36) Schleyer, P. v. R.; Meaerker, C.; Dransfeld, A.; Jiao, H.; Hommes, N. J. R. v. E. *J. Am. Chem. Soc.* **1996**, *118*, 6317.
(37) Chen, Z.; Wannere, C. S.; Corminboeuf, C.; Puchta, R.; Schleyer, P. v. R. *Chem. Rev.* **2005**, *105*, 3842.
(38) Katritzky, A. R.; Barczynski, P.; Musumarra, G.; Pisano, D.; Szafran, M. *J. Am. Chem. Soc.* **1989**, *111*, 7.
(39) Katritzky, A. R.; Karelson, M.; Sild, S.; Krygowski, T. M.; Jug, K. *J. Org. Chem.* **1998**, *63*, 5228.
(40) Jug, K.; Köster, A. M. *J. Phys. Org. Chem.* **1991**, *4*, 163.
(41) Cyrański, M. K.; Krygowski, T. M.; Wisiorowski, M.; Hommes, N. J. R. v. E.; Schleyer, P. v. R. *Angew. Chem., Int. Ed.* **1998**, *37*, 177.
(42) Jusélius, J.; Sundholm, D. *J. Org. Chem.* **2000**, *65*, 5233.
(43) Furuta, H.; Maeda, H.; Osuka, A. *J. Org. Chem.* **2001**, *66*, 8563.
(44) Krygowski, T. M.; Cyrański, M. K.; Czarnocki, Z.; Häfelinger, G.; Katritzky, A. R. *Tetrahedron* **2000**, *56*, 1783.
(45) Wannere, C. S.; Sattelmeyer, K. W.; Schaefer, H. F., III; Schleyer, P. v. R. *Angew. Chem., Int. Ed.* **2004**, *43*, 4200.

Conclusion

A combination of the azulene π-system with the 21,23-dioxaporphyrin-like macrocyclic framework results in formation of dioxadiazuliporphyrin. This carbaporphyrinoid is easily stepwise one-electron oxidizable to its radical cation and, subsequently, to the aromatic dication. During the chemical oxidation, the dioxadiazuliporphyrin redox system exhibits distinct color changes. In general, diheterodiazuliporphyrins are amenable to diverse structural modifications similar to related heteroporphyrins making it easy to fine tune its properties. An example of such controlled modification, presented in detail in this contribution, involves a formal replacement of two sulfur atoms of dithiadiazuliporphyrin by oxygens to yield dioxadiazuliporphyrin. Consequences of this modification have been readily elaborated by a comparison of dioxadiazuliporphyrin and dithiadiazuliporphyrin properties. The inner core alteration seems to result in rather minor overall structural changes. However, in terms of an electronic structure it is important to highlight a fact that a radical and dication of diheterodiazuliporphyrins reveal near-infrared absorptions. Significantly, the replacement of oxygen atom by sulfur in the case of dication yields a remarkable bathochromic relocation of the intense NIR band from 1148 to 1320 nm. At this point, one can comment that the dithiadiazuliporphyrin system provides the lowest energy electronic transitions ever observed for a chromophore confined in the porphyrin-like frame. Thus, diheterodiazuliporphyrins may act as redox-switchable chromophore systems with a potential for electrochromic and molecular conductivity applications.

A dioxadiazuliporphyrin dication reveals structural and ^{1}H NMR features expected of an aromatic [18]annulenoid system. Although a two-electron reduction should yield an antiaromatic [20]annulenoid species, the experimental ^{1}H NMR chemical shifts are consistent with the rather minor, if any, paratropicity of dioxadiazuliporphyrin. The DFT structure optimization carried out for these species followed by NICS and specific chemical shifts calculation are consistent with an experimentally derived conclusion concerning the dioxadiazuliporphyrin electronic structure in function of their oxidation.

Experimental Section

2,5-Bis[(*p*-tolyl)hydroxymethyl]furan was synthesized according to known procedure.[25]

5,10,15,20-Tetra-*p*-tolyl-22,24-dioxadiazuliporphyrinogen 7. 2,5-Bis[(*p*-tolyl)hydroxymethyl]furan (0.175 mmol, 54 mg) and azulene (0.176 mmol, 22.5 mg) were added to dry CH_2Cl_2 (250 mL) under nitrogen. After 15 min, Et_2O/BF_3 (20 μL) was added, and the reaction mixture was protected from light and stirred for the next 40 min. The mixture was evaporated under reduced pressure, and then subjected to chromatography (Al_2O_3, II grade, CH_2Cl_2). The porphyrinogen was eluted as a deep blue fraction. After chromatography, the product was precipitated from CH_2Cl_2 with CH_3OH as bluish powder/crystals. Yield 64 mg, 91%.

^{1}H NMR (C_6D_6, 298 K, 7.16 ppm): δ 8.03 (d, ^3J = 9.7 Hz, 4H), 7.94 (s, 2H), 7.21 (d, ^3J = 7,1 Hz, 8H), 6.95, (t, ^3J = 9.6 Hz, 2H), 6.92 (d, ^3J = 7.6 Hz, 8H), 6.49 (t, ^3J = 9.7 Hz, 4H), 6.22 (s, 4H), 5.92 (s, 4H), 2.05 (s, 12H). ^{13}C NMR (C_6D_6): δ 158.1, 140.2, 137.6, 137.4, 136.6, 136.1, 133.9, 129.6, 129.4, 129.1, 122.2, 109.4, 44.5, 21.0. UV−vis (CH_2Cl_2): λ_{max} (log ϵ) 355 (4.03), 375 (4.00), 529 (2.92), 620 (2.91), 680 (2.81), 752 (2.52). HRMS (ESI, *m*/*z*): 823.35244 (823.35465 for $C_{60}H_{48}O_2Na$ [M + Na]$^+$).

5,10,15,20-Tetra-*p*-tolyl-22,24-dioxadiazuliporphyrin 8. **7** (0.024 mmol, 19 mg) and DDQ (0.096 mmol, 21.8 mg) were dissolved in 50 mL of freshly distilled CH_2Cl_2. The solution was subsequently evaporated under reduced pressure. The product of the reaction, $\mathbf{8}^{2+}$, was then dissolved in 40 mL of freshly distilled THF, and $SnCl_2$ (75 mg) was added. The color of the solution changed from orange-pink to wine-red. The volume of the solution was reduced to 6−8 mL, and the mixture was subjected to chromatography (Al_2O_3, III grade, toluene). The product was eluted as the first fraction, which gave a shiny violet powder after evaporation. The reaction was quantitative, although some amount of the 5,10,15,-20-tetra-*p*-tolyl-22,24-dioxadiazuliporphyrin dication was regenerated during chromatography.

^{1}H NMR (C_6D_6, 298 K, 7.16 ppm): δ 9.54 (s, 2H), 7.73 (d, ^3J = 9.5 Hz, 4H), 7.29 (d, ^3J = 8.1 Hz, 8H), 6.95 (d, ^3J = 7.8 Hz, 8H), 6.80 (s, 4H), 6.68 (t, ^3J = 9.9 Hz, 2H), 6.24 (t, ^3J = 9.9 Hz, 4H), 2.12 (s, 12H). ^{13}H NMR (C_6D_6): δ 157.4, 150.7, 141.2, 139.9, 137.8, 137.4, 136.5, 130.6, 129.3, 128.9, 126.8, 122.9, 112.8, 21.2. UV−vis (CH_2Cl_2): λ_{max} (log ϵ) 406 (4.70), 539 (4.41). HRMS (ESI, *m*/*z*): 796.33286 (796.33358 for $C_{60}H_{44}O_2$, M$^+$).

5,10,15,20-Tetra-*p*-tolyl-22,24-dioxadiazuliporphyrin Dication, $\mathbf{8}^{2+}$. Bromine (20 μL) was added to solution of **8** (0.038 mmol, 30.0 mg) in 50 mL of freshly distilled CH_2Cl_2. The color of the solution changed quickly from dark red to orange-pink. The solid $\mathbf{8}^{2+}\cdot 2[Br_3]^-$ was precipitated by addition of *n*-pentane to the reaction mixture. The reaction was quantitative.

Data for $\mathbf{2}^{2+}\cdot\mathbf{2[Br_3]}^-$. ^{1}H NMR ($CD_3CN$, 298 K, 1.96 ppm): δ 8.90 (s, 4H), 8.17 (br, 8H), 8.10 (t, ^3J = 9.7 Hz, 2H), 8.06 (d, ^3J = 10.0 Hz, 4H), 7.93 (t, ^3J = 9.7 Hz, 4H), 7.76 (d, 8H), 2.70 (s, 12H), −0.39 (s, 2H). UV−vis (CH_2Cl_2): λ_{max} (log ϵ) 416 (4.57), 483 (4.67), 543 (4.83), 680 (4.29), 1148 (4.41). MS (ESI *m*/*z*): 398.145 (389.167 for $C_{60}H_{44}O_2$, M^{2+}). Elemental analysis (%) C, 64.97; H, 3.16; N, 5.57 (calcd for $C_{85}H_{50}Cl_8N_6O_8$ ($\mathbf{8}^{2+}\cdot$DDQ$^{2-}\cdot$2DDQ$\cdot$$CH_2Cl_2$) C, 65.1; H, 3.22; N, 5.36).

Instrumentation. NMR Spectroscopy. ^{1}H and ^{13}C NMR spectra were recorded on a high field spectrometer (^{1}H frequency 500.13 MHz, ^{13}C 125.7 MHz), equipped with a broad-band inverse gradient probehead. Spectra were referenced to the residual solvent signals (chloroform-*d* 7.24 ppm, acetonitrile-d_3 1.96 ppm, benzene-d_6 7.16 ppm). Two-dimensional NMR spectra were recorded with 2048 data points in the t_2 domain and up to 1024 points in the t_1 domain, with a 0.5−1 s recovery delay.

Absorption spectra were recorded on a diode array spectrometer.

Mass spectra were recorded using the electrospray ionization (ESI) technique.

ESR spectra were recorded on the spectrometer operating with X-band equipped with an ER 035 M gaussmeter and an HP 53550B microwave frequency counter. Radical $\mathbf{8}^{\bullet+}$ for the ESR measurement was obtained by addition of $SnCl_2$ in THF to the solution of $\mathbf{8}^{2+}$ in CH_2Cl_2. Progress of the reaction was monitored by UV−vis spectroscopy. Conditions: microwave frequency 9.75602 GHz, microwave power 3.17 mW, modulation amplitude 2.744 T, modulation frequency 100 kHz.

X-ray Analysis. X-ray quality crystals of **7a** were prepared by slow diffusion of methanol into chloroform-*d* solution of **7** (isomers mixture) in a thin tube, and crystals of **8** were obtained by diffusion of heptane into benzene solution of **8** in a thin tube. Data were collected at 100 K. No absorption correction was applied. Crystal data are compiled in Table S1. The structure was solved by direct methods with SHELXS-97 and refined by the full-matrix least-squares method by using SHELXL-97 with anisotropic thermal parameters for non-hydrogen atoms.[46,47]

Electrochemical measurements were performed on a multifunctional electrochemical analyzer using platinum or glassy-carbon disk as a working electrode and platinum wire as the auxiliary electrode. The saturated calomel or silver chloride electrodes were used as the reference electrodes, and they were separated from the bulk

(46) Sheldrick, G. M. *SHELXS97: Program for Crystal Structure Solution;* University of Göttingen: Göttingen, Germany, 1997.

(47) Sheldrick, G. M. *SHELXL97: Program for Crystal Structure Refinement;* University of Göttingen: Göttingen, Germany, 1997.

solution by a glassy diaphragm connected to a bridge filled with the electrolyte solution.

Computational Chemistry. DFT calculations were performed using Gaussian 03.[48] Geometry optimizations were carried out within unconstrained *C*1 symmetry, with starting coordinates preoptimized using semiempirical methods. Becke's three-parameter exchange functional[49] with the gradient-corrected correlation formula of Lee, Yang, and Parr (B3LYP)[50] was used with the 6-31G** basis set. NICS values were calculated at the GIAO-B3LYP/6-31G** level of theory using the B3LYP geometries. Calculations of NMR properties for investigated systems were performed at the B3LYP geometries using the GIAO-B3LYP/6-31G** method.

Acknowledgment. Financial support from the Ministry of Science and Higher Education (Grant PBZ-KBN-118/T09/2004) is kindly acknowledged. Quantum chemical calculations were carried out at the Poznań Supercomputer Center and the Wrocław Supercomputer Center.

Supporting Information Available: Additional computational results (tables and figures) and NMR and crystallographic data. This material is available free of charge via the Internet at http://pubs.acs.org.

JO7015218

(48) Frisch, M. J.; Trucks, G. W.; Schlegel, H. B.; Scuseria, G. E.; Robb, M. A.; Cheeseman, J. R.; Montgomery, J. A., Jr.; Vreven, T.; Kudin, K. N.; Burant, J. C.; Millam, J. M.; Iyengar, S. S.; Tomasi, J.; Barone, V.; Mennucci, B.; Cossi, M.; Scalmani, G.; Rega, N.; Petersson, G. A.; Nakatsuji, H.; Hada, M.; Ehara, M.; Toyota, K.; Fukuda, R.; Hasegawa, J.; Ishida, M.; Nakajima, T.; Honda, Y.; Kitao, O.; Nakai, H.; Klene, M.; Li, X.; Knox, J. E.; Hratchian, H. P.; Cross, J. B.; Bakken, V.; Adamo, C.; Jaramillo, J.; Gomperts, R.; Stratmann, R. E.; Yazyev, O.; Austin, A. J.; Cammi, R.; Pomelli, C.; Ochterski, J. W.; Ayala, P. Y.; Morokuma, K.; Voth, G. A.; Salvador, P.; Dannenberg, J. J.; Zakrzewski, V. G.; Dapprich, S.; Daniels, A. D.; Strain, M. C.; Farkas, O.; Malick, D. K.; Rabuck, A. D.; Raghavachari, K.; Foresman, J. B.; Ortiz, J. V.; Cui, Q.; Baboul, A. G.; Clifford, S.; Cioslowski, J.; Stefanov, B. B.; Liu, G.; Liashenko, A.; Piskorz, P.; Komaromi, I.; Martin, R. L.; Fox, D. J.; Keith, T.; Al-Laham, M. A.; Peng, C. Y.; Nanayakkara, A.; Challacombe, M.; Gill, P. M. W.; Johnson, B.; Chen, W.; Wong, M. W.; Gonzales, C.; Pople, J. A. *Gaussian03*, revision C.02; Gaussian, Inc.: Wallingford, CT, 2004.

(49) Becke, A. D. *Phys. Rev. A* **1988**, *38*, 3098.

(50) Lee, C.; Yang, W.; Parr, R. G. *Phys. Rev. B* **1988**, *37*, 785.